COMPACT POWER CONDITIONING AND RF SYSTEMS FOR A HIGH POWER RF SOURCE

K. A. O'Connor* and R. D. Curry
University of Missouri-Columbia
Columbia, Missouri 65211

L. Altgilbers
U.S. Army Space and Missile Defense Command/Army Forces Strategic Command
Huntsville, Alabama

ABSTRACT

High power RF systems have increasing potential for application by the Army. High power RF, or high power microwave (HPM), systems can disrupt or disable enemy communications and weapons systems. Fundamental constraints on the availability of HPM sources to the war fighter are the size and portability. Traditional pulsed power systems capable of producing high power RF signals are massive and stationary, making their implementation on the battlefield impractical. Additionally, most systems are powered by the electrical grid. Therefore, research has been required to custom design components that are small, lightweight, portable, and use an independent energy source. The resulting system will be able to produce HPM from a compact package that can be delivered by a variety of means and remotely activated.

1. INTRODUCTION

The University Consortium for High Power Microwave Integration was a collaborative effort between Texas Tech University (TTU), the University of Missouri-Columbia (MU), and the University of New Mexico. The consortium was formed to advance the technology of the components required for a compact HPM source with the final goal of full system integration, resulting in a radiated HPM signal. The system's compact energy source was a flux compression generator (FCG), a high energy device that converts the energy of explosives into a high power electrical signal, which was investigated by TTU. MU focused on power conditioning components used to modulate the output of the FCG into a high voltage, high frequency RF signal.

The relatively long current output pulse from an FCG must be conditioned to create a high power RF burst. The Center for Physical and Power Electronics at the University of Missouri-Columbia developed several compact pulsed power components and integrated a full RF system. The system consists of a non-magnetic core, spiral-wound transformer and an exploding wire fuse as its fundamental elements. A crowbar switch was added to limit the effects of stray inductance and prevent excessive voltages across the fuse. The RF source consists of a high voltage, low inductance capacitor and a low inductance closing switch and shunt. An antenna in parallel with the RF load can then radiate the RF signal.

In addition to the power conditioning and RF systems, an experimental test stand was constructed to simulate the input of an FCG. The FCG simulator produces inexpensive, repeatable, and non-destructive testing of the power conditioning and RF systems in non-explosive experiments. Extensive testing of the full system has been performed with the FCG simulator. Experiments have included optimization of the power conditioning components and trials of multiple RF load geometries. This paper will provide an overview of the system operation, detail the FCG simulator and each of the crucial components, and review progress in recent experimental tests.

2. SYSTEM OPERATIONAL OVERVIEW

The full power conditioning system is an augmented version of a system proposed by Reinovsky, Lindermuth, and Vorthman (Reinovsky et al., 1989). The augmented system investigated at UMC is pictured in Fig. 1.

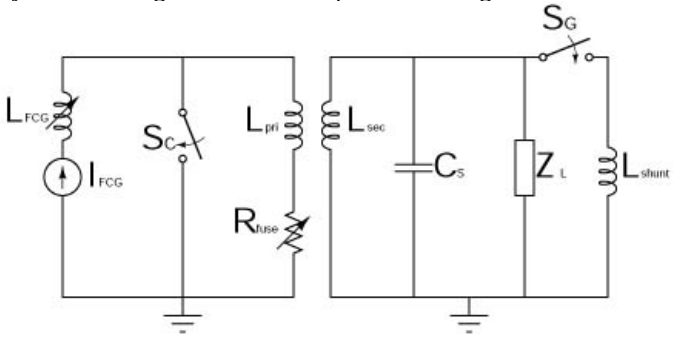

Fig. 1 Schematic of a current source and power conditioning system

The circuit was originally designed to be driven by a flux compression generator (FCG) or, for non-destructive testing purposes, an FCG simulator. The current source is represented schematically in Fig. 1 as a variable inductance, L_{FCG}, through which a current, I_{FCG}, flows.

Report Documentation Page

Form Approved
OMB No. 0704-0188

1. REPORT DATE	2. REPORT TYPE	3. DATES COVERED
DEC 2008	**N/A**	**-**

4. TITLE AND SUBTITLE	5a. CONTRACT NUMBER
Compact Power Conditioning And Rf Systems For A High Power Rf Source	5b. GRANT NUMBER
	5c. PROGRAM ELEMENT NUMBER
6. AUTHOR(S)	5d. PROJECT NUMBER
	5e. TASK NUMBER
	5f. WORK UNIT NUMBER
7. PERFORMING ORGANIZATION NAME(S) AND ADDRESS(ES) **University of Missouri-Columbia Columbia, Missouri 65211**	8. PERFORMING ORGANIZATION REPORT NUMBER
9. SPONSORING/MONITORING AGENCY NAME(S) AND ADDRESS(ES)	10. SPONSOR/MONITOR'S ACRONYM(S)
	11. SPONSOR/MONITOR'S REPORT NUMBER(S)

12. DISTRIBUTION/AVAILABILITY STATEMENT
Approved for public release, distribution unlimited

13. SUPPLEMENTARY NOTES
See also ADM002187. Proceedings of the Army Science Conference (26th) Held in Orlando, Florida on 1-4 December 2008, The original document contains color images.

14. ABSTRACT

15. SUBJECT TERMS

16. SECURITY CLASSIFICATION OF:			17. LIMITATION OF ABSTRACT	18. NUMBER OF PAGES	19a. NAME OF RESPONSIBLE PERSON
a. REPORT	b. ABSTRACT	c. THIS PAGE			
unclassified	**unclassified**	**unclassified**	**UU**	**8**	

The core elements of the power conditioning system consist of the pulse transformer, represented by L_{pri} and L_{sec}, and the exploding wire fuse opening switch, R_{fuse}. The closing switch, S_C, is the crowbar switch, added to limit excessive voltages from appearing across the fuse due to L_{FCG} or any stray circuit inductances. Additionally, a load capable of producing high power RF to be radiated by an antenna was built and tested. The load consists of a low inductance, high voltage capacitor, C_S, a low inductance shunt, L_{shunt}, a self-breaking closing switch, S_G, and an antenna or dummy load, Z_L.

System operation can be described in three stages. The first stage corresponds to operation of the FCG or FCG simulator. As the current input to the power conditioning system increases, the energy is inductively stored in the inductance of the pulse transformer. At the same time, resistive heating of the fuse brings the fuse wires to the point of vaporization. The time of the first stage of system operation is the risetime of the current from the FCG or FCG simulator, which is usually 6 – 12 μs. At the conclusion of the first stage of operation, the current from the source has reached its maximum, and the inductance of the FCG or FCG simulator is at a minimum. The second stage of operation corresponds with the fuse wires reaching vaporization, resulting in a dramatic increase in fuse resistance. The rise in fuse resistance results in a fast decrease of current in the primary circuit. The flux change in the transformer windings as the primary current falls causes large voltages across the transformer terminals and an energy transfer to the secondary circuit. The capacitor across the transformer secondary terminals, C_S, is charged to high voltage. The end of the second stage of operation occurs when the switch on the secondary, S_G, closes due to an overvoltage condition. Ideally, the closing of the secondary switch also corresponds with the primary current reaching zero. During the third stage of operation, the high voltage capacitor forms an underdamped oscillator with the shunt inductance, L_{shunt}. An RF signal is thus applied across the antenna or dummy load, Z_L, which can then be radiated or dissipated as desired.

3. FCG SIMULATOR

An on-campus test stand was necessary for the several power conditioning components to be repeatedly and cost-effectively tested. The test stand was designed to produce the nearly exponential current rise of an FCG. Unlike a simple capacitive discharge in which the peak current occurs at zero dI/dt, it is desired that the current reach the desired peak value while the rate of current rise is still high. Two methods of simulating this waveform were demonstrated by Belt, and a system based upon magnetically switched parallel inductors was built at MU (Belt, 2006).

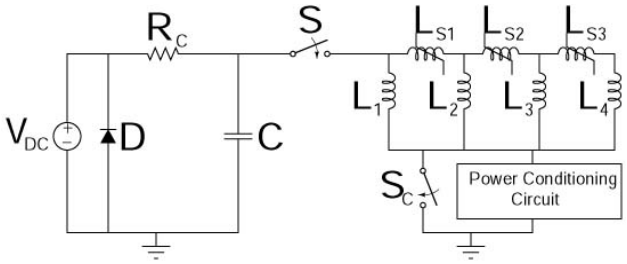

Fig. 2 Basic schematic of FCG simulator with power conditioning components and crowbar switch

Figure 2 above displays the basic schematic for the FCG simulator. A high voltage capacitor is discharged through the network of parallel inductors in which $L_1 > L_2 > L_3 > L_4$. The inductors L_{S1}, L_{S2}, and L_{S3} are saturating magnetic cores that sequentially switch the parallel inductors into the circuit. The MU simulator is designed to drive an external inductive load, specifically the transformer inductance. Therefore, the simulator at MU was designed to have a minimal inductance after all of the cores had saturated. Figure 3 shows the FCG simulator during initial testing.

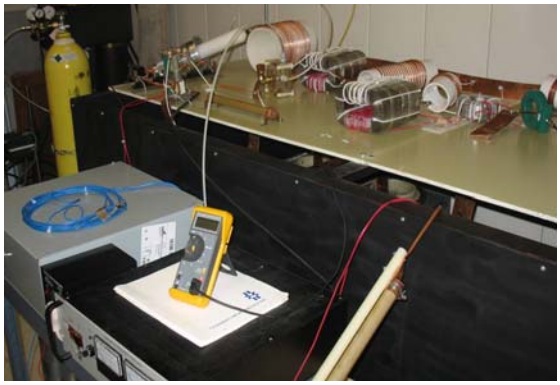

Fig. 3 FCG Simulator

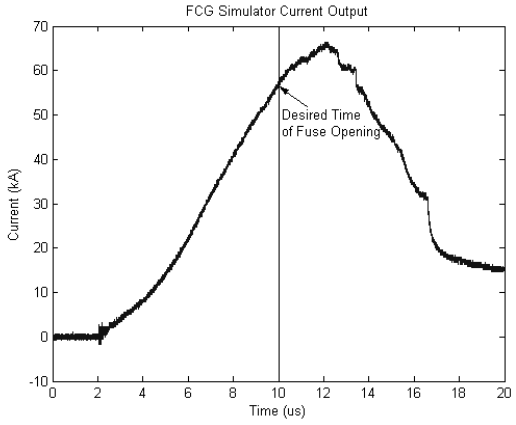

Fig. 4 Current waveform from FCG simulator

Figure 4 shows a typical current rise from the FCG simulator, demonstrating the effect of the decreasing circuit inductance on the rate of current rise. A current rise time in the range of 8-10 μs was desired to replicate

the expected FCG input. The vertical line placed 8 μs after the beginning of current rise represents the time at which the fuse would be designed to vaporize. The data in Fig. 4 was taken without a transformer or fuse load, resulting in a peak current after 8 μs between 55 kA and 60 kA. The addition of the power conditioning components typically reduces this peak current to between 30 kA and 40 kA.

4. POWER CONDITIONING COMPONENTS

4.1 Pulse Transformer

The pulse transformer was designed following the concepts of Martin and Rohwein (O'Loughlin, 1988). The transformers utilized a spiral-strip geometry with a non-magnetic core. The windings were made of tapered copper foils and mylar insulating sheets. The outer diameter of the transformers is approximately 15.24 cm, and the length of the transformers is approximately 17.78 cm.

The FCGs produced for this system were designed to operate into microhenry loads, so the minimum transformer primary self-inductance was designed to be 1 μH. A turns ratio of 1:3 was chosen to allow the transformer-fuse components to drive a low impedance RF load if necessary. The coupling factor is decreased due to the use of a non-magnetic core transformer, but coupling factors up to .85 have been achieved with the present construction techniques. The step-up ratio could be increased for capacitive loads while only minimally increasing the leakage inductance. Figure 4 shows an example transformer.

Fig. 5 Spiral-strip pulse transformer

4.2 Exploding Wire Fuse

The opening switch was implemented as a two-section array of parallel wires. Between 15 and 36 wires are typically used, depending on the desired action integral before opening. Forty gauge silver-plated copper wires with a 6.1% plating thickness were chosen based on previous fuse wire studies (Neuber, 2005).

The wires are angled in each of the two sections of the fuse. Copper field shapers provide the form on which the wires are angled. The spacing between the top and bottom field shapers ranged from 15.24 cm to 30.48 cm, depending on the required fuse voltage holdoff. The entire assembly was packaged in a 15.24 cm cylinder with very fine glass beads as a quenching medium. The glass beads were rated with a mesh size of 170-325.

Fig 6. Fuse is shown with wires and field shapers (left). The fuse is packed with fine glass beads (right).

4.3 Crowbar Switch

The inductance of an FCG is a minimum at the end of its operation, at the peak current output. As previously mentioned, the FCG simulator was designed to also have a minimal inductance at the time of peak current. However, experiments proved that the inductance of the FCG simulator at the time of fuse opening was non-negligible. As a result, there was a very significant additional voltage across the fuse as the current was interrupted. The resulting restrike on many of the experiments did not allow complete system operation. It was determined that a crowbar switch was required to divert the excess energy stored in the stray inductance. With the crowbar switch in place, the voltage across the fuse at the time of the fuse opening should approximately equal the voltage across the transformer primary winding. The crowbar switch was implemented as a simple atmospheric pressure air spark gap. The spacing of the switch was adjusted between 1 cm and 2 cm to ensure that the spark gap did not close before the fuse opened.

5. HIGH POWER RF CIRCUIT

The prototype high voltage capacitor used for initial system testing was capable of holding off voltages of several hundred kilovolts and oscillating at frequencies of

hundreds of megahertz. However, the first prototype was built as a tri-plate capacitor, which is an inconvenient geometry for compact portable systems. Therefore, the capacitor had to be redesigned to conform to the geometry and size constraints to which the pulse transformer and exploding wire fuse were built. Specifically, the capacitor would have to be redesigned for a cylindrical geometry with a diameter less than or equal to 15.24 cm. Two cylindrical geometries are described in this paper.

5.1 Spiral-Strip Geometry

Given the results of the spiral-strip pulse transformers in the tests reported in previous experiments, several aspects of the design and construction of the new cylindrical capacitor were borrowed from those proven by the pulse transformer. First, stacks of thin dielectric films are used as insulation to allow for the capacitor to be wound around a cylindrical core. Second, the high voltage connection is made along the center axis of the cylinder to adequately distance the high voltage input terminal from the ground foil and provide a direct coaxial connection with the high voltage output of the pulse transformer.

If a stack is formed adjacent to the core outer diameter with the HV foil, dielectric layer, ground foil, and additional dielectric layer, the stack can be rolled around a cylindrical core to form a cylindrical capacitor. When the length of the foils is larger than the circumference of the first winding, the additional windings will form a rolled tri-plate capacitor, increasing the electrical energy storage in a given volume.

The capacitor was wound on a 30.5 cm long cylindrical core with approximately a 7.75 cm diameter. The width of the high voltage foil was approximately 22.75 cm, and the length was 61 cm. Ten Teflon® films of 508 µm thickness each were wound between the capacitor foils for a total dielectric thickness per layer of 5.08 mm. The outer diameter of the wound capacitor was within the 15.24 cm limit. The predicted capacitance, assuming a relative dielectric constant of 2.1, is 850 pF. The measured capacitance with the capacitor submerged in oil was approximately 730 pF. The difference between the predicted and measured values is largely a result of the increased distance between foils where the winding was loose. The capacitance increase from the tri-plate prototype to the present cylindrical version was 265%. Fig. 7 shows the wound capacitor, and Fig. 8 displays the arrangement of the capacitor with the pulse transformer and other load components.

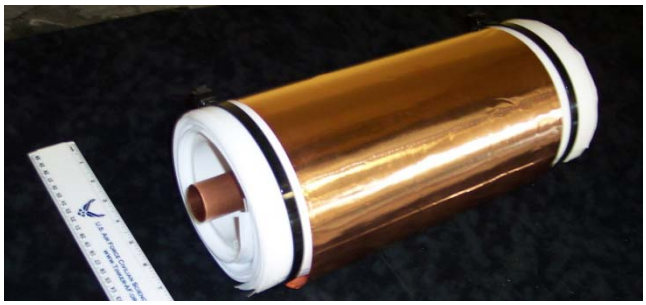

Fig. 7 Cylindrical capacitor with axial high voltage connection.

Fig. 8 Full system load with pulse transformer at upper left.

5.2 Coaxial Cylinder Geometry

The third high voltage capacitor geometry, the coaxial cylinder geometry, was designed and tested as another candidate for the high frequency RF load. The geometry has advantages of a cylindrical form, a center axis high voltage connection, a small diameter, and the use of oil as the bulk dielectric medium. Additionally, the construction of the capacitor is much more easily performed than the winding of the films for the spiral-strip capacitor. The coaxial cylinder capacitor is formed by aligning conducting cylinders along the same cylindrical center axis. Each successive cylinder has a larger radius and opposite electrical polarity to the previous cylinder. The cylinder with the smallest radius is at HV polarity as it is directly connected with the axial high voltage output of the pulse transformer. The cylinder with the largest radius is at ground potential, which is ideal for encasing the system or for placing adjacent to the ground plane in the experimental setup.

The capacitance of coaxial cylinders has been thoroughly studied for their common use as transmission lines (Ulaby, 2001). With the multiple capacitive layers of the coaxial cylinder geometry, the equation for a single coaxial structure can be expanded to give the total capacitance. *R1*, *R2*, *R3*, and *R4* are the cylinder radii with $R1 < R2 < R3 < R4$.

$$C = 2\pi\varepsilon_0\varepsilon_r l\left[\frac{1}{\ln\left(\frac{R2}{R1}\right)}+\frac{1}{\ln\left(\frac{R3}{R2}\right)}+\frac{1}{\ln\left(\frac{R4}{R3}\right)}\right] \quad (1)$$

As previously stated, one of the advantages of the coaxial cylinder geometry is the relative ease of construction compared with a wound capacitor. Each of the conducting cylinders was formed by affixing a single layer of copper foil to a PVC pipe of known diameter. For cylinders with radii *R2*, *R3*, and *R4*, a copper tab protruded from the cylinder for electrical connection. For high voltage insulation, the tab from the cylinder with radius *R3* was placed on the opposite side as the tabs from cylinders with radii *R2* and *R4*. The cylinders were held in place by insulators and threaded rods. To reduce the inductance of the oscillating circuit, the oil spark gap switch was connected directly to the tabs of the capacitor. Two prototype coaxial cylinder capacitors are seen in Fig.

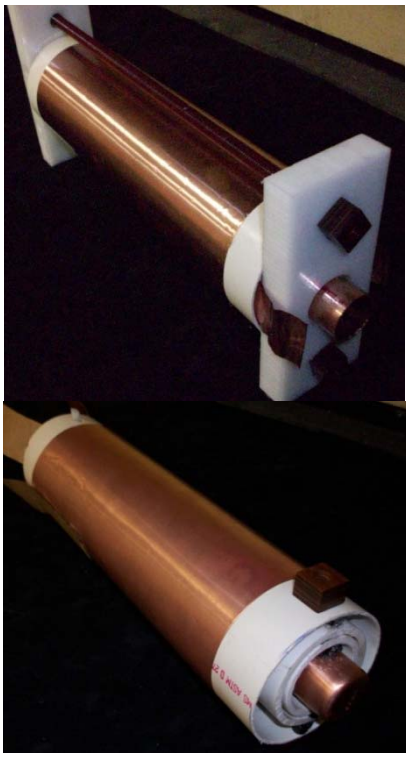

Fig. 9 Assembled coaxial cylinder capacitors

The outer diameter of the largest cylinder is 8.23 cm, making the coaxial cylinder the most compact geometry investigated here. The predicted capacitance based on equation (1) is 337 pF. However, the measured capacitance in oil was higher at 459 pF. Upon disassembling the capacitor after testing, it was determined that the oil affected the adhesive used to affix the foils to the PVC piping, resulting in the foil at radius *R2* detaching from the outer diameter of the pipe it was affixed to and unwinding to the inner radius of the larger pipe. The effective increase of the radius *R2* greatly reduced the distance between adjacent foils and could explain the unexpectedly high capacitance value. As this foil movement also puts the capacitor at much greater risk for dielectric breakdown at high voltage, an improved method of affixing the foils to the piping is required for future designs.

6. EXPERIMENTAL RESULTS

Many experiments were conducted to optimize the various power conditioning components. Final tests were aimed at full system operation with a current input similar to that expected from an FCG. An antenna was not used in the experiments being presented in this paper. A resistive load that approximates the impedance of free space radiation was used in place of an antenna. The experimental setup is shown in Fig. 6.

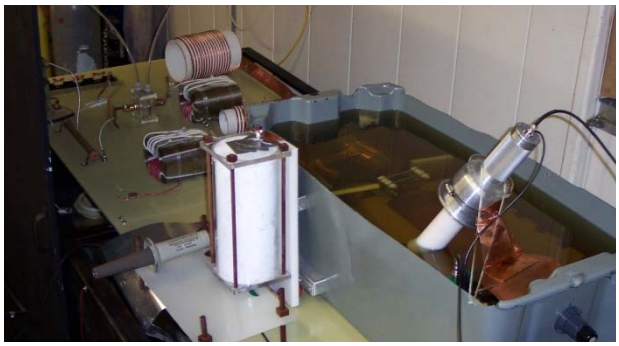

Fig. 10 Integrated test setup: Power conditioning components at lower right with FCG simulator at upper left.

Experiments with the original tri-plate capacitor geometry were successful in both reaching very high load voltages and oscillating at very high frequencies on the order of 10s to 100s of MHz. Results of RF power levels reaching over 130 MW with the FCG simulator have been previously reported, and power levels reaching more than 250 MW have been recorded (O'Connor and Curry, 2007). Experiments driven by FCGs have reached load charging voltages greater than 700 kV, and fields of 6 kV/m peak-to-peak have been measured at a distance of 5.5 m from the experimental setup (Holt et al., 2007). The experiments presented here with cylindrical capacitors were meant to produce similar results with the much more compact load capacitors.

6.1 Spiral-Strip Geometry

As a part of the experiments with the spiral-strip capacitor, lower input energies were used to demonstrate the effectiveness of the system with smaller energy sources. In previously reported experiments, the peak primary current was 32 kA, corresponding to an

inductively-stored energy of 512 J (O'Connor and Curry, 2007). However, at the time when the oil gap closed with a capacitor voltage of 200 kV, the primary current was 20 kA. The corresponding 200 J of inductively-stored energy remaining was therefore extraneous. To reduce wasted energy, a lower energy source of 312 J might have been used to achieve the same results with the oil gap closing at peak voltage just as the primary current reaches zero amps. An inductively-stored energy of 312 J corresponds to a primary current of about 25 kA. Therefore, currents around 25 kA were desired for the experiments with the spiral-strip capacitor.

Experimental tests of the complete system with spiral-strip capacitor were conducted with the FCG simulator at MU. A water resistor of 384 Ω was implemented as a dummy load for Z_L and as a voltage divider for capacitor voltage measurements. Since the power conditioning system was driven with much lower currents than in previous studies, the number of fuse wires was reduced to 17 40-gauge silver-plated copper wires. A crowbar switch, S_C, was included to limit the effects of the inductance of the FCG simulator during the fuse resistance rise.

Figs. 11 and 12 show results for full power conditioning system operation. Fig. 11 shows the current in the transformer primary and fuse opening switch. The FCG simulator drives the primary current to a peak of approximately 25 kA in a risetime of approximately 10 μs. As the fuse resistance rapidly rises, the primary current falls from 22.5 kA to zero in 200 ns. Oscillations of the secondary circuit result in large oscillations of the primary current about zero.

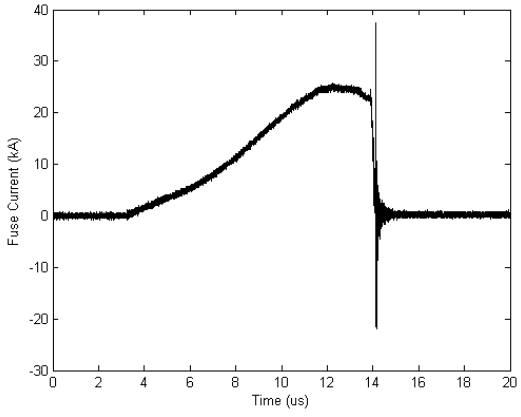

Fig. 11 Full View of Primary Current Waveform

Fig. 7 gives a detailed view of the high voltage stages of load operation. The capacitor charged to -190 kV before the oil spark gap closed to form an underdamped RLC circuit with the shunt inductance. Several very high frequency oscillations are present before a series of lower frequency oscillations. With the parallel resistive load across the capacitor of 384 Ω, the peak load power was greater than 90 MW.

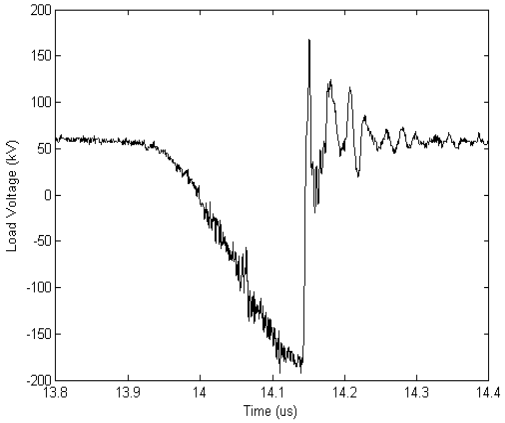

Fig. 12 Detailed View of Load Voltage RF Oscillations

The peak values from a Fast Fourier Transform (FFT) analysis on the waveform in Fig. 12 occur at 2.5 MHz, corresponding to the capacitor charging. The most significant frequency component of the secondary oscillations occurs at 40 MHz. There is significant frequency content up to about 75 MHz. Additional frequency components around 200 MHz form the upper frequency limit. After the load capacitor has been fully charged, the load oscillation frequency content is mostly in the range from 30 MHz to 75 MHz. Therefore, this iteration of the load is considered a mesoband oscillator. Including the frequency content down to 2.5 MHz during capacitor charging, the load is considered a hyperband oscillator (Giri and Tesche, 2006).

The peak capacitor charging voltage was only slightly lower to those previously reported in for the tri-plate design despite the capacitance increase. The inductively-stored energy for this experiment with a peak current of 25 kA was 312.5 J. Compared to the previous experiment with a peak current of 32 kA and corresponding inductively-stored energy of 512 J, the inductively-stored energy was reduced by 39%. The ability to achieve similar peak charging voltages on a larger capacitance despite significantly reduced input energy demonstrates the compatibility of the power conditioning system and oscillating load with lower energy sources.

A possible component failure is dielectric breakdown in the compact high voltage capacitor. Nevertheless, this component failure can also result in successful overall system operation. In this case, the capacitor is shorted by dielectric failure before the oil spark gap closes. However, as seen in the detailed view of Fig. 13, this situation also results in high frequency voltage oscillations. In an experiment with a primary current of 28.5 kA, dielectric breakdown occurred at about -190 kV, which is believed

to be due to air remaining between the dielectric layers. The subsequent peak reached 225 kV, corresponding to 130 MW. An FFT of the oscillations shows the peak frequency component to be 2.5 MHz, corresponding to capacitor charging, with frequency content up to 75 MHz. This situation demonstrates that for single-shot systems, the dielectric breakdown of the capacitor can also produce the high frequency load oscillations desired.

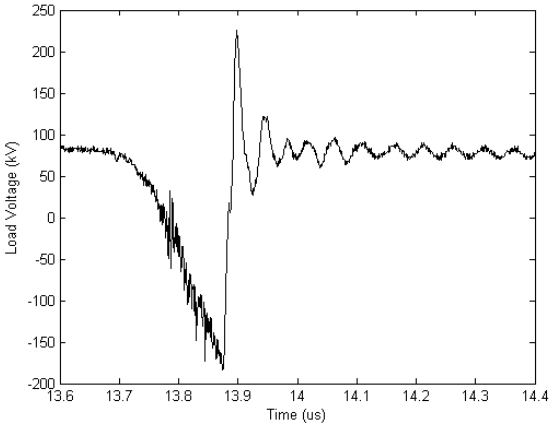

Fig. 13 Detailed view of load voltage after dielectric breakdown

Another fault mode of operation occurs if the oil spark gap does not close. The relatively high value of the fuse resistance at this point in system operation allows the approximation of the inductance parallel to the capacitor to be the secondary self-inductance. This inductance is much higher than the shunt inductance. Nevertheless, the system secondary circuit will oscillate at a lower frequency. A wideband antenna can still radiate high power RF despite the incomplete system operation. It is seen as an advantage of the system that two of the most common load failures still result in high power RF generation.

6.2 Coaxial Cylinder Geometry

The final geometry tested for the RF load was the coaxial-cylinder capacitor. The tests with this capacitor were driven by the MU FCG simulator. In parallel with the coaxial-cylinder capacitor was a resistive load of 540 Ω, which provided a divider for high voltage measurements and a load to substitute for a radiating antenna. The pulse transformer and fuse form were identical to those used in the tests of the spiral-strip capacitor. The fuse consisted of 18 40-gauge silver-plated copper wires in parallel. The capacitance in oil of the coaxial-cylinder capacitor was 459 pF.

Figure 14 shows the detailed primary current waveforms. The current rose to a peak of approximately 27 kA in about a 10 μs risetime. The current was then rapidly reduced from 25 kA to about 5 kA in approximately 150 ns. The inductively-stored energy of 5 kA in the primary when the RF oscillations began was approximately 12.5 J, so relatively little inductively-stored energy was wasted.

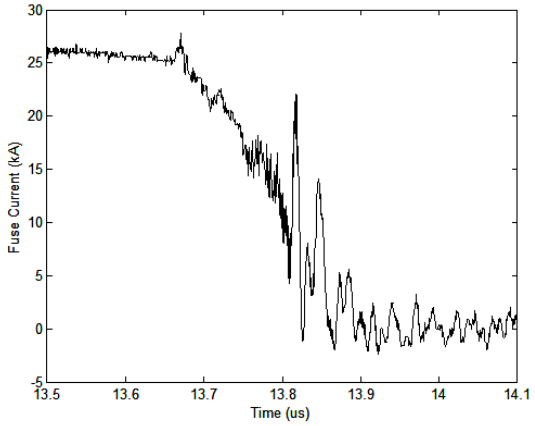

Fig. 14 Detailed view of primary current in test of coaxial-cylinder RF load

Figures 15 and 16 show the full and detailed load voltage waveforms. As the fuse resistance rises and energy is transferred to the secondary circuit, the load capacitor was charged to approximately -180 kV. At this point, a breakdown occurred that resulted in high power load oscillations. The peak RF power reached approximately 70 MW. The power rating is lower due to the higher load resistance used in this experiment. The breakdown that resulted in the RF oscillations was within the capacitor, so the system operation for this experiment was similar to the failure mode presented in the previous subsection. It is believed that the breakdown within the capacitor occurred due to the ineffective adhesives in oil. As previously described, one of the inner foils came off of the pipe it had been affixed to, which greatly reduced the gap between the free foil and the adjacent foil. Therefore, future coaxial-cylinder capacitors must use adhesives or other mechanisms that are resistant to oil.

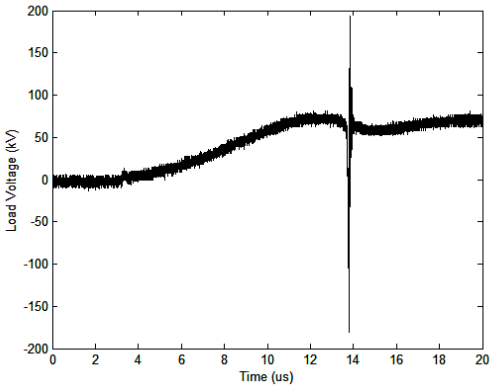

Fig. 15 Full view of load voltage for coaxial-cylinder RF load

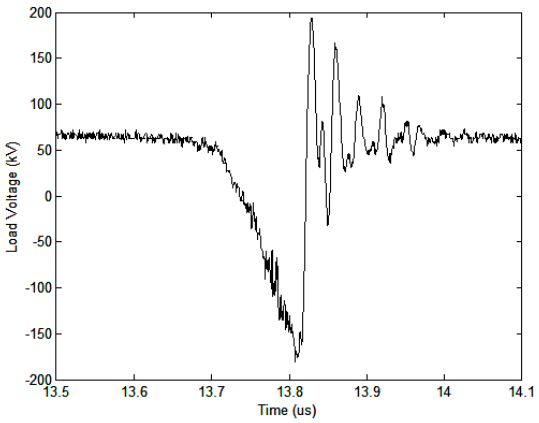

Fig. 16 Full view of load voltage for coaxial-cylinder RF load

An FFT analysis of the waveform of Fig. 16 reveals there is very high content less than 40 MHz as well as a substantial wide peak from 50 MHz to 70 MHz. These wide frequency bands could be radiated by a wideband antenna. The peak frequencies may be limited by the oscillating circuit forming within the capacitor rather than the preferred low inductance path through the oil switch. Eliminating the dielectric breakdown in the capacitor and lowering circuit inductances could increase the peak frequencies towards those observed with the tri-plate geometry.

CONCLUSIONS

Several power conditioning and RF components have been developed to provide a compact and portable source of high power RF signals. A pulse transformer, exploding wire fuse, and crowbar switch were developed as power conditioning components that could be adapted to drive multiple HPM loads. Each component was designed and built to fit within a 15.24 cm cylindrical form. The development of a compact RF oscillator was focused on the geometry of a capacitor capable of holding off hundreds of kilovolts. The spiral-strip capacitor was developed from the concepts of the previously-successful spiral-strip transformer. The spiral-strip geometry was built to the 15.24 cm specification with a capacitance of 730 pF. The coaxial cylinder capacitor was designed with the advantages of relative simplicity and a very small diameter. The coaxial cylinder capacitor was built with a capacitance of 459 pF in a diameter of only 8.23 cm.

Experiments included integrated tests of the FCG simulator, power conditioning system, and new cylindrical RF systems. The spiral-strip based RF system reached peak voltages of greater than 190 kV and 225 kV with corresponding peak powers of 90 MW and 130 MW. Significant frequency content was present in the RF signal around 2.5 MHz and from 30 to 75 MHz with additional content around 200 MHz. The RF system based on the coaxial cylinders reached load voltages greater than 180 kV with a corresponding power of 70 MW. Both of the cylindrical RF systems demonstrate the potential for achieving a high power RF radiating system in a compact package, and research into system improvements is continuing.

The technologies presented in this paper illustrate the potential for adapting pulsed power components into compact packages. The improved portability of HPM systems will allow their use by future war fighters to disable or disrupt an enemy's use of electronics and electromagnetic communication systems. The complete system could be small and portable enough to be delivered as a short range projectile or carried by a soldier.

REFERENCES

Belt, D., 2006: Non-explosive test bed for flux compression generator fuses. Thesis, Electrical and Computer Engineering Department, Texas Tech University, 95 pp.

Holt, T. *et al*, 2007: Investigation of an FCG and pulse transformer based power conditioning system. *Proc. of the 16th IEEE International Pulsed Power Conference*, Albuquerque, NM, IEEE, CD-ROM.

Giri, D.V., and Tesche, F.M., 2004: Classification of intentional electromagnetic environments (IEME). *IEEE Transactions on Electromagnetic Compatibility*, 46, 322-328.

Neuber, A.A. (Ed.), 2005: *Explosively Driven Pulsed Power*. 1st Edition. Springer-Verlag, 280 pp.

O'Connor, K.A., Curry, R.D., 2007: Investigation of a high voltage, high frequency power conditioning system for use with flux compression generators. *Proc. of the 16th IEEE International Pulsed Power Conference*, Albuquerque, NM, IEEE, CD-ROM.

O'Loughlin, J.P., Sidler, J.D., Rohwein, G.J., 1988: Air core pulse transformer design. *Conf. Record of the 1988 18th Power Modulator Symposium*, IEEE, p. 325-330.

Reinovsky, R.E., Lindemuth, I.R., and Vorthman, J.E., 1989: High voltage power condition systems powered by flux compression generators. *Proc. of the 7th Pulsed Power Conference*, IEEE, p. 971-974.

Ulaby, F.T., 2001: *Fundamentals of Applied Electromagnetics*. 3rd Edition. Prentice Hall, 433 pp.